Human Molecular Genetics, 2006, Vol. 15, No. 16 **2509–2522**
doi:10.1093/hmg/ddl172
Advance Access published on July 6, 2006

Compound heterozygosity for mutations in *LMNA* causes a progeria syndrome without prelamin A accumulation

Valerie L.R.M. Verstraeten[1,4,*], Jos L.V. Broers[3,5,6], Maurice A.M. van Steensel[1,4], Sophie Zinn-Justin[7], Frans C.S. Ramaekers[3,4,5], Peter M. Steijlen[1,4], Miriam Kamps[1,3,4], Helma J.H. Kuijpers[3], Diane Merckx[2], Hubert J.M. Smeets[2], Raoul C.M. Hennekam[8,9], Carlo L.M. Marcelis[10] and Arthur van den Wijngaard[2]

[1]Department of Dermatology and [2]Department of Clinical Genetics, University Hospital Maastricht, The Netherlands, [3]Department of Molecular Cell Biology, [4]Research Institute for Growth and Development (GROW) and [5]Cardiovascular Research Institute Maastricht (CARIM), University of Maastricht, The Netherlands, [6]Department of Biomechanics and Tissue Engineering, Faculty of Biomedical Engineering, Technical University of Eindhoven, The Netherlands, [7]Département d'Ingénierie et d'Etudes des Protéines, CEA Saclay, France, [8]Institute of Child Health, University College London, UK, [9]Department of Pediatrics, Academic Medical Center, University of Amsterdam, The Netherlands and [10]Department of Clinical Genetics, Radboud University Nijmegen Medical Centre, The Netherlands

Received March 21, 2006; Revised and Accepted June 5, 2006

***LMNA*-associated progeroid syndromes have been reported with both recessive and dominant inheritance. We report a 2-year-old boy with an apparently typical Hutchinson–Gilford progeria syndrome (HGPS) due to compound heterozygous missense mutations (p.T528M and p.M540T) in *LMNA*. Both mutations affect a conserved region within the C-terminal globular domain of A-type lamins, defining a progeria hot spot. The nuclei of the patient showed no prelamin A accumulation. In general, the nuclear phenotype did not correspond to that previously described for HGPS. Instead, honeycomb figures predominated and nuclear blebs with reduced/absent expression of B-type lamins could be detected. The healthy heterozygous parents showed similar nuclear changes, although in a smaller percentage of nuclei. Treatment with a farnesylation inhibitor resulted in accumulation of prelamin A at the nuclear periphery, in annular nuclear membrane plaques and in intra/trans-nuclear membrane invaginations. In conclusion, these findings suggest a critical role for the C-terminal globular lamin A/C region in nuclear structure and support a major contribution of abnormal assembly to the progeroid phenotype. In contrast to earlier suggestions, we show that prelamin A accumulation is not the major determinant of the progeroid phenotype.**

INTRODUCTION

Hutchinson–Gilford progeria syndrome (HGPS) is a rare genetic disorder that leads to premature aging and is characterized by abnormalities in skin, bone, fat tissue, hair and blood vessels (1,2). Affected children have a shortened life expectancy, mainly due to heart failure as a consequence of atherosclerosis and extensive fibrosis. HGPS resembles mandibuloacral dysplasia (MAD) to a large extent. The early onset of disease and its rapid progression differentiate HGPS from MAD. In addition, the persistence of scalp hair, the less obvious lipodystrophy and more pronounced osteolysis in distal phalanges, clavicles and mandible are more typical for MAD. Children with HGPS have a typically beaked nose with broad nose bridge and prominent vein signature.

Recently, a *de novo* heterozygous mutation (c.1824C>T, p.G608G) in the *LMNA* gene was identified in HGPS (3,4). The *LMNA* gene encodes lamins A, C, AΔ10 and C2, which

*To whom correspondence should be addressed at: Department of Dermatology, University Hospital Maastricht, P. Debyelaan 25, PO Box 5800, 6202 AZ Maastricht, The Netherlands. Tel: +31 433875641; Fax: +31 433877293; Email: vve@sder.azm.nl

© *The Author 2006. Published by Oxford University Press. All rights reserved.*
For Permissions, please email: journals.permissions@oxfordjournals.org

Downloaded from https://academic.oup.com/hmg/article/15/16/2509/645147 by guest on 24 April 2024

belong to the intermediate filament protein family and consist of an N-terminal head domain, an α-helical rod domain that is important in dimerization and a mostly globular C-terminal tail domain suggested to be of importance in the interaction with several nuclear components such as emerin and Lap2α (5). Lamins are involved in maintenance of nuclear integrity, DNA replication and gene expression [reviewed in (6)]. Mature lamin A is produced by processing of prelamin A and lacks the C-terminal 18 amino acids predicted by the cDNA sequence. Prelamin A contains a C-terminal CaaX (cysteine-aliphatic-aliphatic-other)-box motif that undergoes a series of post-translational processing steps. These include farnesylation at the CaaX cysteine followed by proteolytic removal of the a-a-X motif, carboxyl methylation of the terminal cysteine and a second proteolytic cleavage step removing the last 15 C-terminal amino acids from the precursor. Mutations in nuclear lamins cause a group of disorders that are collectively referred to as laminopathies (7). So far, at least eight different laminopathies have been associated with autosomal dominant/recessive mutations in *LMNA*, including Emery–Dreifuss muscular dystrophy type 2, limb girdle muscular dystrophy type 1b, dilated cardiomyopathy type 1A, Dunnigan-type familial partial lipodystrophy, Charcot–Marie–Tooth disease type 2B1, MAD, HGPS and restrictive dermopathy (RD). Mutations in *ZMPSTE24*, a zinc metalloproteinase involved in the processing of prelamin A, have been associated with several progeroid syndromes (8–10).

The *de novo* heterozygous p.G608G truncating mutation in *LMNA* was found in 18 out of 20 classical HGPS patients (4). The mutation results in a c.1824C>T (p.G608G) transversion in exon 11 and activates a cryptic donor splice site at position c.1819 (3). Lamin A products in these patients consist of mature lamin A and progerin, a 50 amino acid deleted lamin A protein that remains farnesylated (11). Wild-type lamin A was shown to be more tightly associated with its nuclear-binding sites in the presence of progerin, as concluded from fluorescence recovery after photobleaching experiments (12). Morpholino antisense RNA blocking of the cryptic splice site induced by the G608G mutation resulted in rescue of the nuclear and cellular phenotype of wild-type lamin A as well as the normalization of expression of several genes dysregulated in HGPS (12). These experiments support a dominant negative effect of progerin in classical HGPS. In non-classical progeria syndromes, due to *LMNA* or *ZMPSTE24* mutations, an accumulation of prelamin A was found in the nuclei of the patients (10,13). The presence of prelamin A in the nuclear lamina was predicted to disturb the nuclear structure and cause the severe progeroid phenotype (10). Moreover, treatment with a farnesyltransferase inhibitor (FTI) could rescue the nuclear phenotype in patients with a progeroid syndrome by localizing prelamin A away from the lamina into the nucleoplasm (14,15). This finding suggests that prelamin A has effects comparable to those of progerin. Interestingly, the FTI could relocalize progerin in a similar way, resulting in a striking improvement of nuclear morphology in HGPS fibroblasts (14,16).

Here, we describe a 2-year-old boy with an apparently typical HGPS caused by compound heterozygous mutations in *LMNA* resulting in p.T528M and p.M540T. Both parents are heterozygous for a mutation in *LMNA* and clinically unaffected, although a considerable percentage of their fibroblasts exhibit dysmorphic nuclei. The nuclear abnormalities found in the patient's fibroblasts differ from those associated with classical HGPS. Prelamin A accumulation could not be detected in the 2-year-old, but treatment with a farnesylation inhibitor induced prelamin A accumulation organized at the nuclear rim, in annular nuclear membrane plaques and in intra/trans-nuclear membrane invaginations.

RESULTS

Clinical characteristics of the index patient

The proband (Fig. 1) was born after an uneventful pregnancy with a normal birth weight (3120 g). His mother and father, aged 33 and 38, respectively, were both healthy. Until the age of 1 year, the child developed normally, but thereafter developed a failure to thrive and showed hair loss. At the age of 2, all his growth parameters had decreased significantly (height −4 SD, weight −2.5 SD, head circumference −2 SD). The patient showed the classical features of HGPS: sparse hair growth with areas of alopecia, prominent veins, prominent forehead, mild proptosis, narrow nasal bridge with a prominently visible vein, still full cheeks and small mouth (Fig. 1A and B). Lipodystrophy was noticed, in addition to prominent large joints and a horse-riding stance. The distal phalanges were significantly shortened and showed a thickened and reddened skin (Fig. 1C).

Radiography showed a vertical skull base, Wormian bones and dental crowding (Fig. 2A). The distal phalanges showed osteolysis and tufting (Fig. 2B) and the distal ends of the clavicles exhibited translucency typical of osteoresorption (Fig. 2C).

Compound heterozygosity for mutations in the LMNA gene

Two heterozygous missense mutations were found in the proband: c.1583C>T (p.T528M) in exon 9 inherited from the father and c.1619T>C (p.M540T) in exon 10 inherited from the mother. A clinically unaffected younger sister was found to have the c.1583C>T mutation. Both mutations affect the C-terminal globular domain of A-type lamins (discussed subsequently).

Immunohistochemical lamin staining patterns

Fibroblasts of patient and parents were obtained by a skin biopsy and used for immunohistochemical analysis at passages 3 and 4. In all three subjects, irregularly shaped nuclei with blebs, honeycomb figures, large and poorly defined protrusions and intra/trans-nuclear tubule-like structures could be detected. In control fibroblasts blebbing and honeycomb figures could be detected in about 2 and 3% of the nuclei, respectively. All nuclei were counterstained with propidium iodide (PI).

Staining with the lamin A antibody 133A2 (Fig. 3A1–3), the lamin A/C antibody Jol-2 (Fig. 3B1–3) and the lamin C antibody RalC (Fig. 3C1–3) revealed honeycomb figures in the nuclear lattice and its protrusions in ∼36% of all nuclei

Downloaded from https://academic.oup.com/hmg/article/15/16/2509/645147 by guest on 24 April 2024

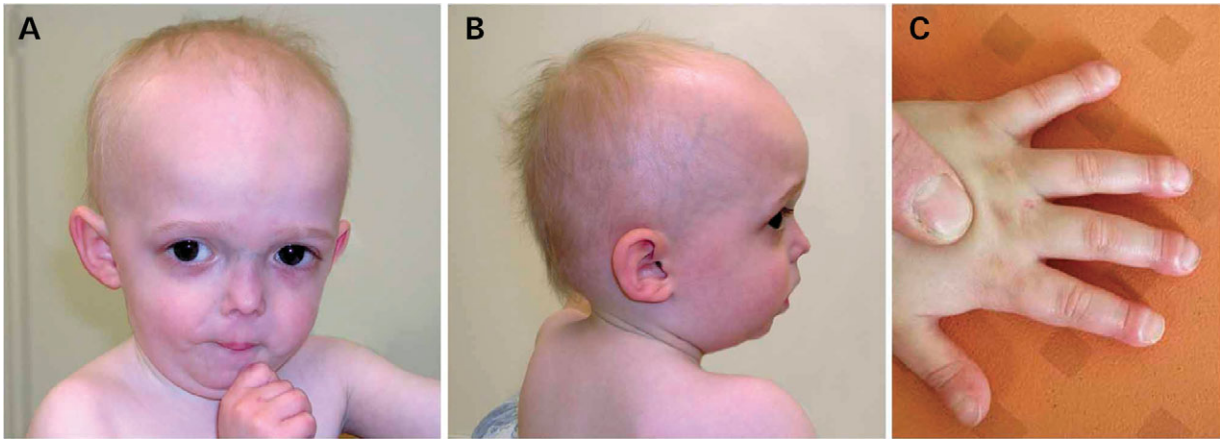

Figure 1. Clinical characteristics in the proband at 2 years. (**A** and **B**) Frontal bossing, sunken eyes with sparse eyelashes and eyebrows, a beaked nose with a prominent vein on top and a small mouth are clearly visible. There is a retro-micrognathia. The scalp shows a taut skin with prominent veins, sparse hair growth on the occipital and parietal regions and alopecia of the frontal part of the scalp. (**C**) Broadened and shortened distal phalanges with reddening of the skin.

in the patient (arrows in Fig. 3A1 and B1) and in ~6% of the nuclei from the mother and father. A-type lamins remained present in the lamina lining the nuclear blebs, detected in ~20% of the patient's nuclei and in ~6% of the parents' nuclei. Farnesylation inhibition by lovastatin in these cells resulted in an overall improvement of the nuclear phenotype by diminishing the number of honeycomb structures and blebbing. In the case of the patient, the number of honeycomb structures and nuclear blebbing was reduced from 36 and 20%, respectively to 10% each. Intra/trans-nuclear tubules could be detected. Inhibition of farnesylation increased the number of nuclear membrane invaginations per nucleus significantly (Table 1).

Immunostaining for the inner nuclear membrane protein emerin (Fig. 3D1–3) revealed nuclear lamina localization, a faint signal in the cytoplasm and honeycomb patterns in both patient and parents. A more intense emerin signal could be detected in the lamina of most nuclear blebs (arrows in Fig. 3D1 and 3).

Immunostaining with 119D5-F1 for lamin B1 (Fig. 4A1–3) and with LN43 for lamin B2 (Fig. 4B1–3) showed honeycomb patterns and reduced to absent expression of B-type lamins in the lamina lining the nuclear protrusions (arrows in Fig. 4A1, B1 and B3).

Immunostaining for prelamin A with the α-PA antibody revealed an absent or poor lamina signal in human control fibroblasts NHDFα (Fig. 5A, passage 8), fibroblasts from a patient with classical HGPS due to a p.G608G mutation (Fig. 5D, passage 9), in the patient fibroblasts (Fig. 5G, passage 7) and cell cultures from his parents (data not shown). Treating the control fibroblasts (Fig. 5B and C), HGPS fibroblasts (Fig. 5E and F) and those from the patient (Fig. 5H, I, M and N) with 40 μM lovastatin resulted in prelamin A accumulation at the nuclear rim, in well-organized intra/trans-nuclear membrane invaginations (detailed three-dimensional view given by the stereo projections in Fig. 5M) and at annular nuclear membrane plaques from which tubules project into the nucleoplasm (detailed three-dimensional view given by the stereo projections in Fig. 5N and by the orthogonal view in Fig. 5N′) (Table 1). Few of these annular plaques did not track further into the nucleoplasm and seemed to remain as plaque structures at the nuclear surface. The nucleoplasm was devoid of prelamin A labeling. PI counterstaining showed no apoptosis-related features in these nuclei. Fibroblasts of a patient with RD due to homozygous c.1085_1086insT truncating mutations in *ZMPSTE24* were used as a control for the prelamin A staining (Fig. 5J–L). Here, similar percentages of nuclei with tubular and plaque structures could be detected with the prelamin A antibody before (Fig. 5J, passage 10) and after (Fig. 5K and L) lovastatin treatment. Inhibition of farnesylation increased the number of nuclear membrane invaginations per nucleus significantly in the patient and control, but no significant increase could be detected in the patient with HGPS (data not shown) and in the patient with RD (Table 1). The increase in nuclear membrane invaginations detected by the Jol-2 antibody was even more obvious in a staining for prelamin A (Table 1). Some cells revealed a granular prelamin A staining pattern in the cytoplasm, both before and after farnesylation inhibition (Fig. 5A and C).

Immunohistochemical analysis of patient fibroblasts after farnesylation inhibition by FTI-277

Fibroblasts of the 2-year-old index patient (passage 15) and control fibroblasts (NHDFα, passage 8) were studied for the presence of nuclear membrane invaginations after 18 h incubation with the FTI-277 (20 μM). Staining with the prelamin A antibody α-PA revealed accumulation of prelamin A at the nuclear rim and in multiple intra/trans-nuclear membrane invaginations in patient (Fig. 5O) and control cells (data not shown). These tube-like structures resemble those observed in fibroblasts treated with lovastatin (40 μM for 18 h). Donut-shaped nuclei could be found. Apoptosis-related abnormalities could not be detected by PI counterstaining. The number of intra/trans-nuclear membrane invaginations increased significantly after farnesylation inhibition by FTI-277 (Table 1).

Downloaded from https://academic.oup.com/hmg/article/15/16/2509/645147 by guest on 24 April 2024

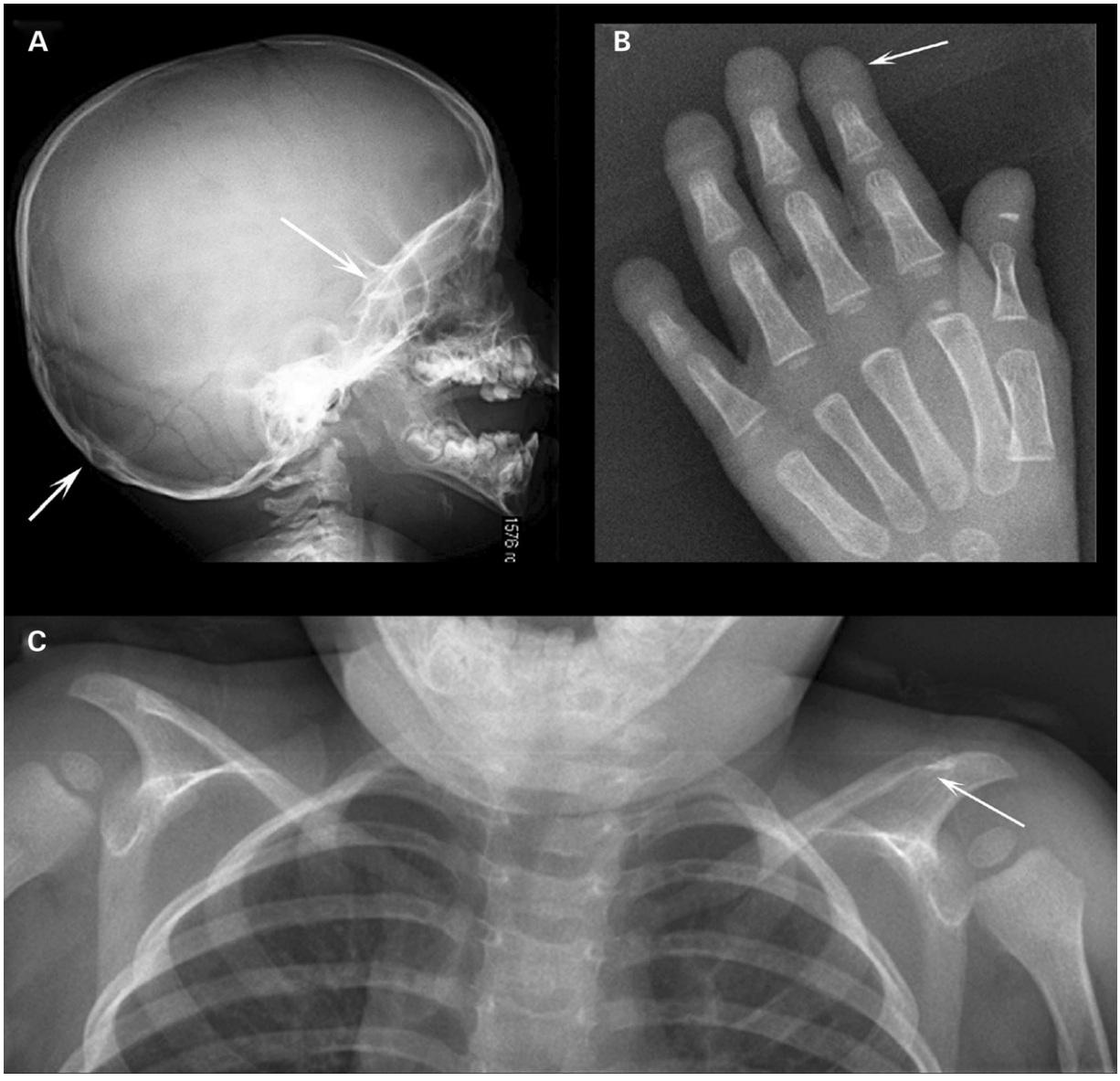

Figure 2. Radiography in the proband at 2 years. (**A**) Skull with vertical base (arrow) and Wormian bones in the occipital region (arrow). (**B**) Hand with decreased bone density and shortening of the distal phalanges, consistent with acro-osteolysis (arrow). (**C**) Chest radiography showing translucency of the distal parts of the clavicles (arrow).

Electron microscopy of cultured patient cells treated by lovastatin

Ultrathin sections from fibroblasts of the 2-year-old index patient (passage 8) were studied by electron microscopy for nuclear membrane invaginations after 18 h of incubation with 40 μM lovastatin (Fig. 6A–C). Heterochromatin was normally organized at the nuclear envelope (NE). Apoptosis-related condensation of chromatin could not be observed. In the nucleoplasm, multiple tube-like structures lined by a double membrane could be detected. These tubes enclosed polyribosomes (Fig. 6C, arrow) and were surrounded by heterochromatin at the nucleoplasmic side, compatible with intra-nuclear membrane invaginations (Ni). Similar structures of variable size could be detected in close relationship to nucleoli (Nu) and nuclear organizer regions (NoR) (Fig. 6A and B, arrows). The number of nuclear membrane invaginations per nucleus was significantly higher in these lovastatin-treated nuclei when compared with non-treated patient nuclei.

Viability assays of lovastatin-treated patient and control fibroblasts

Fibroblasts of the index patient (passage 12) were cultured on glass cover slips in 12-well culture plates and treated with lovastatin at variable concentrations (5–10–20 and 40 μM) for 18 and 42 h. After 18 h, ∼1% PI-positive cells could be detected at all concentrations used. After 42 h, a large part of the patient cells detached from the bottom of the well,

Downloaded from https://academic.oup.com/hmg/article/15/16/2509/645147 by guest on 24 April 2024

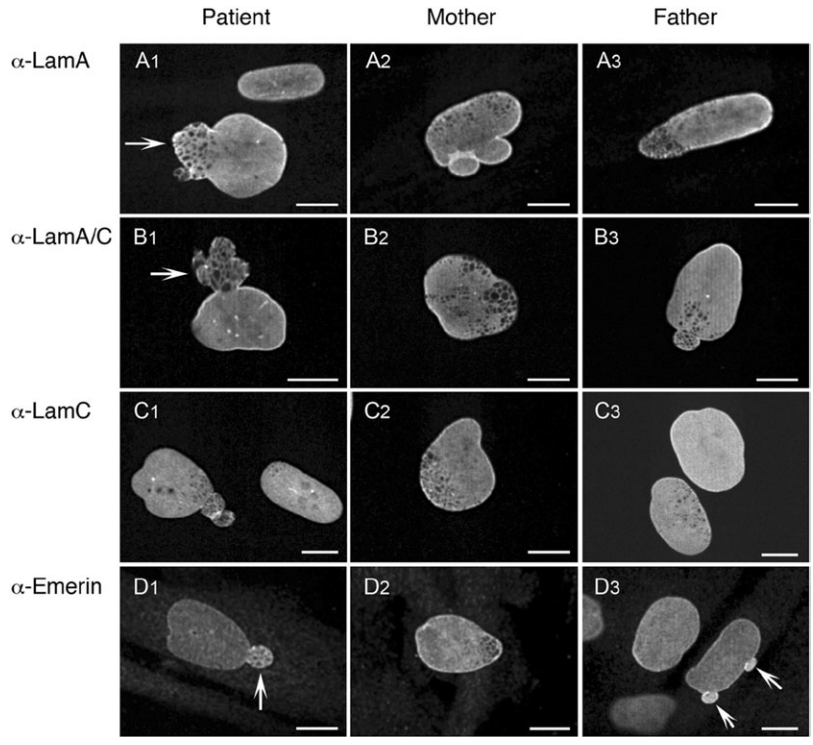

Figure 3. Immunofluorescence labeling in single confocal sections of A-type lamins and emerin in cultured fibroblasts of the patient, mother and father with the lamin A antibody 133A2 (**A**1–3), the lamin A/C antibody Jol-2 (**B**1–3) and the lamin C antibody RalC (**C**1–3). Note the honeycomb pattern in all subjects often located within the protrusions of the nuclei (e.g. Fig. 3A1 and B1, arrows). Blebbing was a common finding in all subjects (e.g. Fig. 3A2 and B3). Note that A-type lamins remain present in these blebs. Staining with the emerin antibody NCL-Emerin (**D**1–3) showed the same honeycomb pattern and blebbing (e.g. Fig. 3D1 and 3, arrows). The expression of emerin seemed increased within the blebs of most nuclei. A weak expression of emerin was often detected in the cytoplasm. Scale bars represent 10 μm.

Table 1. Frequence of trans/intra-nuclear membrane invaginations in control and patient fibroblasts before and after farnesylation inhibition

	Cell line	Farnesylation inhibition	% of cells with more than five nuclear membrane invaginations	% of cells with less than five nuclear membrane invaginations
Jol-2	NHDFα	−	9.7 ± 5.8	32.7 ± 12.4
	NHDFα	+ Lovastatin	27.7 ± 7.4	27.7 ± 11.8
	2-year-old patient	−	11.3 ± 1.1	34.6 ± 4.6
	2-year-old patient	+ Lovastatin	29 ± 8.4	15.5 ± 2.1
	RD	−	38.5 ± 4.9	40 ± 9.8
	RD	+ Lovastatin	43.5 ± 0.7	35.5 ± 0.7
α-PA	NHDFα	+ Lovastatin	49.7 ± 7.5	24 ± 14.2
	NHDFα	+ FTI-277	56 ± 2.8	21.5 ± 3.5
	2-year-old patient	+ Lovastatin	53.5 ± 9.0	20.5 ± 7.9
	2-year-old patient	+ FTI-277	64 ± 1.4	8.5 ± 2.1
	RD	−	30 ± 5.6	50.5 ± 4.9
	RD	+ Lovastatin	31 ± 5.6	52.5 ± 6.3

A specification of nuclear morphology encountered in control fibroblasts (NHDFα), the fibroblasts of the 2-year-old patient and a patient with RD due to a homozygous c.1085_1086insT mutation in *ZMPSTE24*. By use of the lamin A/C antibody, Jol-2 and the prelamin A antibody α-PA cells were evaluated for the presence of trans/intra-nuclear membrane invaginations before (−) and after inhibition of farnesylation by lovastatin (40 μM for 18 h) or FTI-277 (20 μM for 18 h). With the lamin A/C antibody, the number of nuclear membrane invaginations per nucleus was found to be increased after farnesylation inhibition. The increase in nuclear membrane invaginations was even more obvious with the prelamin A antibody α-PA. Average percentages from two or more experiments in which each 100 cells were counted are given with standard deviation.

and in all concentrations used ∼60% of the total cell population was non-viable, as judged from nuclear PI-labeling. In an additional experiment fibroblasts of the index patient (passage 13) and control fibroblasts (NHDFα, passage 6) were cultured in six-well culture plates, treated with lovastatin (40 μM) for 18 and 42 h, and subsequently analysed by a fluorescence-activated cell sorting (FACS) assay to quantitate the number of non-viable cells. After 18 h, ∼2% and after

Downloaded from https://academic.oup.com/hmg/article/15/16/2509/645147 by guest on 24 April 2024

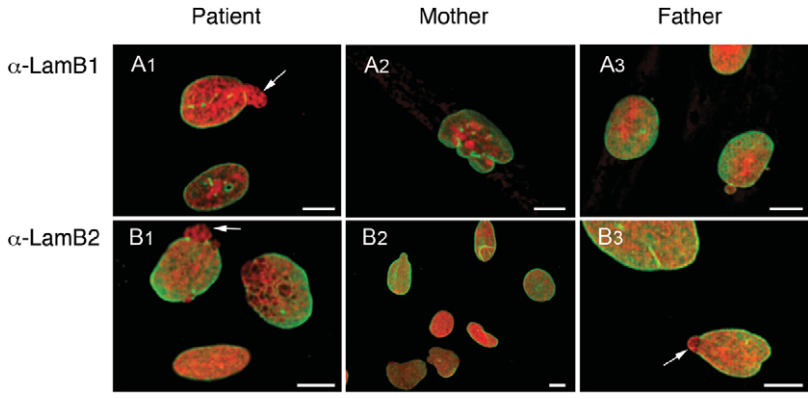

Figure 4. Immunofluorescence labeling of B-type lamins (green) of cultured fibroblasts of the proband, mother and father with the lamin B1 antibody 119D5-F1 (**A**1–3) and the lamin B2 antibody LN43 (**B**1–3). The nuclei were counterstained with PI (red). Note that in all cell cultures nuclei could be detected with chromatin protrusions that were not encapsulated by B-type lamins (arrows in A1, B1 and B3). Scale bars represent 10 μm.

42 h ~16% of the total cell population of patient and control were PI-permeable. The effect of lovastatin was more pronounced when cells were cultured on glass cover slips instead of plastic.

Immunoblotting for A-type lamins

We performed immunoblotting for A-type lamins (Fig. 7) with fibroblasts from the patient (lane1), his mother (lane 2) and father (lane 3), the patient with RD (lane 4), the control human fibroblast cell line (NHDFα) (lane 5) and the patient with classical HGPS due to the p.G608G mutation (lane 6). Actin was used as a loading control. With the prelamin A antibody α-PA, no signal could be observed in the protein samples of the patient, his parents, control fibroblasts or HGPS, whereas a distinct prelamin A band could be detected in the RD patient (Fig. 7A, compare lanes 1–3 with lane 4). This band could also be detected with the Jol-2 and X67 antibodies (Fig. 7B and C, respectively, lane 4) as a band having a slightly increased molecular weight when compared with lamin A. With the Jol-2 antibody, recognizing the C-terminal globular domain of A-type lamins (Fig. 7B), lamins A and C were positively identified, next to a third band below lamin C identifying the 46 kDa proteolytic fragment containing the C-terminal end of lamins A/C generated during the homogenization process (17) (asterisk). No significant differences in expression levels between the normal and mutant lamins were observed. Also, the lamin A/C ratio seemed to be largely unaltered. These findings were confirmed using the lamin A/C antibody X67, recognizing the N-terminal domain of A-type lamins (Fig. 7C).

Interestingly, no distinct band could be detected with the prelamin A antibody in the protein sample of the patient with classical HGPS. This indicates that the prelamin A antibody does not detect progerin, the truncated product that evolves from the use of the cryptic splice-site induced by the p.G608G mutation. The prelamin A antibody recognizes the last 15 amino acids of prelamin A of which progerin lacks the −aaX motif as well as the first seven amino acids of the epitope recognized by the prelamin A antibody. However, with the X67 antibody, an additional band could be found in between lamins A and C, most likely representing progerin (Fig. 7C, lane 6, double asterisk). This band could not be detected with the Jol-2 antibody, suggesting that although the 50 amino acid deletion in progerin does not affect the epitope of Jol-2 (i.e. amino acids 464–572), the deletion may abolish epitope recognition. A schematic illustration of the epitopes recognized by the different antibodies used in the immunoblotting assay is given (Fig. 7D).

Three-dimensional structure of the A-type lamin C-terminal Ig-fold

The three-dimensional structure of the C-terminal Ig-like domain (411–553) of A-type lamins was determined by NMR spectroscopy (18) and X-ray crystallography (19). The affected residue T528 is located on β-strand 8 next to residue R527 involved in MAD (p.R527H) (20) and in a progeria syndrome (p.R527C) (21); its side chain is buried in the hydrophobic core of the domain (Fig. 8A and C). Residue M540 is solvent accessible and located on β-strand 9 of the same β-sheet, close to residue K542 associated with a progeria syndrome (p.K542N; Fig. 8A and C) (22). The three-dimensional representation reveals that all these residues are close to each other (Fig. 8B). They are also close to residue R471, mutated into cysteine in a progeria syndrome (21).

In conclusion, residues R471, R527, T528, M540 and K542 define a hot spot for mutations causing progeria-like diseases. Whereas the buried residues R471 and T528 are well conserved in all lamins (as indicated by their dark blue color in Fig. 8A and C), the solvent-exposed residues R527, M540 and K542 (depicted in green in Fig. 8A–C) are conserved in A-type lamins but not in B-type lamins. The hot spot defined by these residues is distinct from the positively charged surface highly conserved in A- and B-type lamins and affected in FPLD (e.g. residues K486 and R482) (Fig. 8B).

DISCUSSION

Here, we present a case of apparently typical HGPS without prelamin A accumulation resulting from compound heterozygous mutations in the *LMNA* gene, consisting of

Downloaded from https://academic.oup.com/hmg/article/15/16/2509/645147 by guest on 24 April 2024

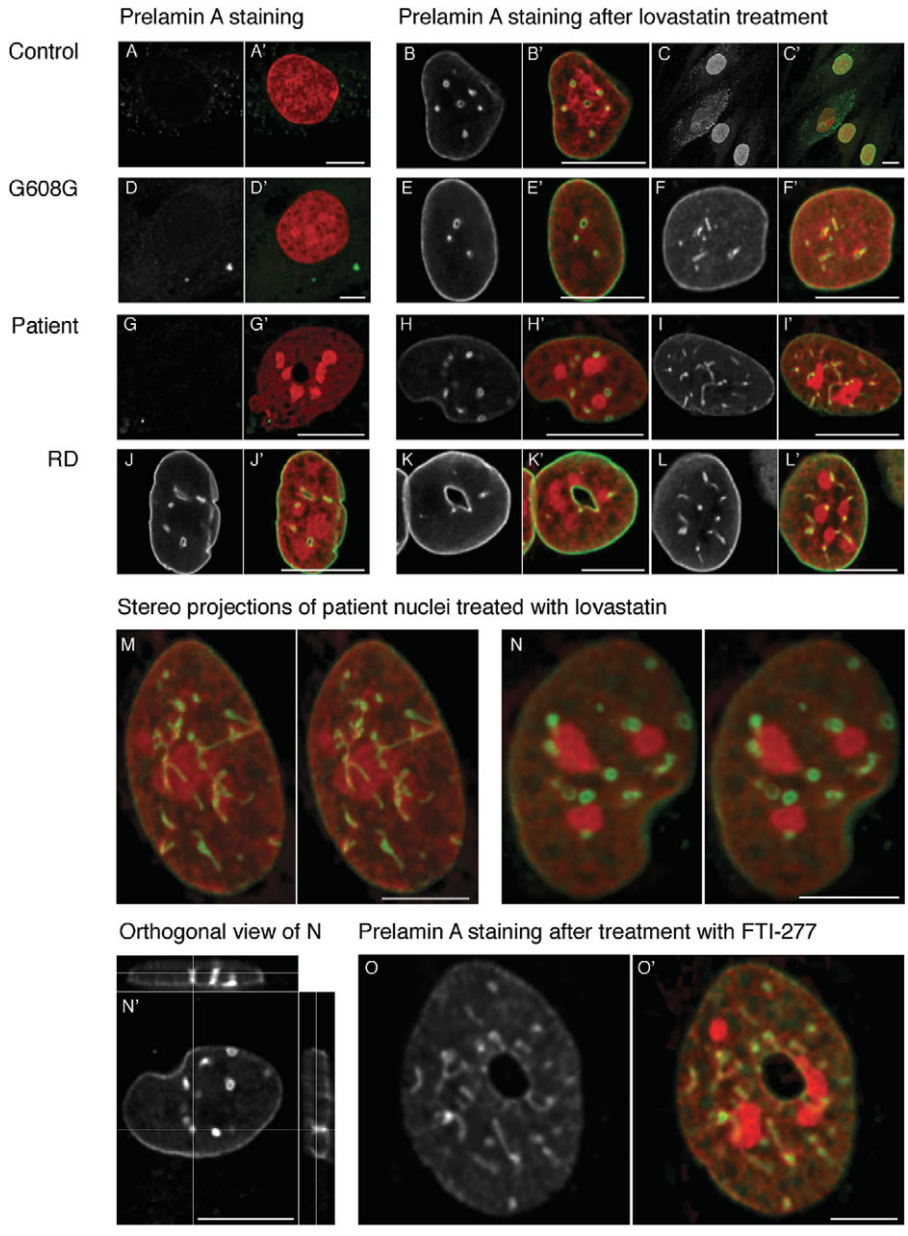

Figure 5. Prelamin A staining [**A**–**L**, **N**′ and **O**; green fluorescence in (A′–L′, **M**, N and O′)] of cultured fibroblasts before and after inhibition of farnesylation. All nuclei were counterstained with PI [red fluorescence in (A′–L′, M, N and O′)]. Prelamin A staining revealed absent to very weak lamina signals in normal human dermal fibroblasts NHDFα (A), in fibroblasts from a patient with classical HGPS due to a p.G608G mutation (D) and in fibroblasts from the 2-year-old index patient (G). Fibroblasts of a patient with an RD caused by a homozygous c.1085_1086insT mutation in *ZMPSTE24*, predicted to result in an inactive truncated protein, revealed prelamin A accumulation at the nuclear rim, in intra/trans-nuclear membrane invaginations and in annular nuclear membrane plaques (J). Farnesylation inhibition by lovastatin resulted in a similar prelamin A accumulation pattern in NHDFα (B and C) and in the fibroblasts of HGPS (E and F) and the 2-year-old patient (H, I, M and N). The prelamin A expression pattern remained largely unaltered in the RD patient after lovastatin treatment (K and L). A detailed view on the nuclear membrane invaginations is given by the stereo projections in (M). A detailed view on the annular nuclear membrane plaques from which nuclear membrane invaginations project into the nucleoplasm is given by the stereo projections in (N). Some of the nuclear invaginations result in trans-nuclear tubules as demonstrated in the orthogonal view (N′). Treatment of patient fibroblasts with the FTI-277 (20 μM for 18 h) resulted in a similar pattern of prelamin A accumulation. Prelamin A predominantly accumulated in tube-like structures (O). Donut-shaped nuclei could be detected (O). Scale bars represent 10 μm.

p.T528M in combination with a novel mutation p.M540T. The early onset of disease, its progression, the pronounced alopecia, the beaked nose with prominent nasal bridge and vein on top and the enlarged knee joints are characteristic for HGPS. The pronounced acro-osteolysis is a signature symptom for MAD and makes the HGPS phenotype in our patient slightly atypical. However, the osteolysis of the distal ends of the clavicles and neurocranium is mild and similar to that found in other HGPS patients. The overall phenotype is largely reminiscent of classical HGPS.

The p.M540T mutation inherited from the apparently healthy mother has not been described before and is located

Downloaded from https://academic.oup.com/hmg/article/15/16/2509/645147 by guest on 24 April 2024

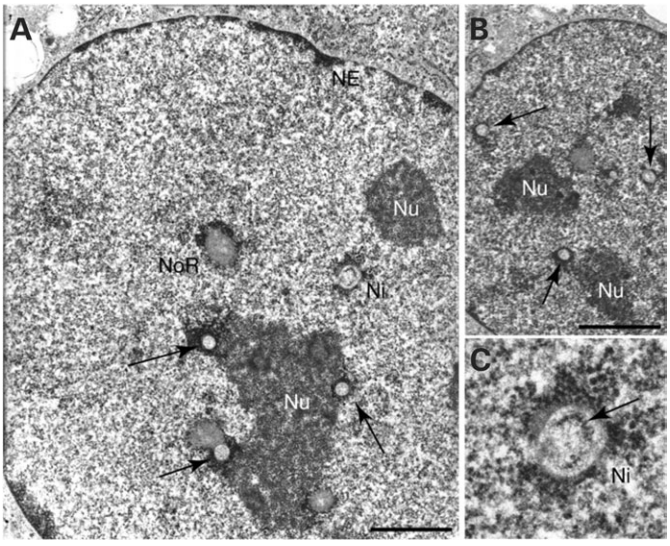

Figure 6. Electron microscopy of ultrathin sections from the index patients' fibroblasts treated with lovastatin (40 μM for 18 h) revealed multiple intranuclear double-membrane lined structures, enclosing polyribosomes (arrow in **C**) and surrounded by heterochromatin at the nucleoplasmic side, indicating the existence of nuclear membrane invaginations (Ni). Similar structures of variable size could be detected in close relationship to nucleoli (Nu) and nuclear organizer regions (NoR) [arrows in (**A** and **B**)]. Scale bars correspond to 1 μm.

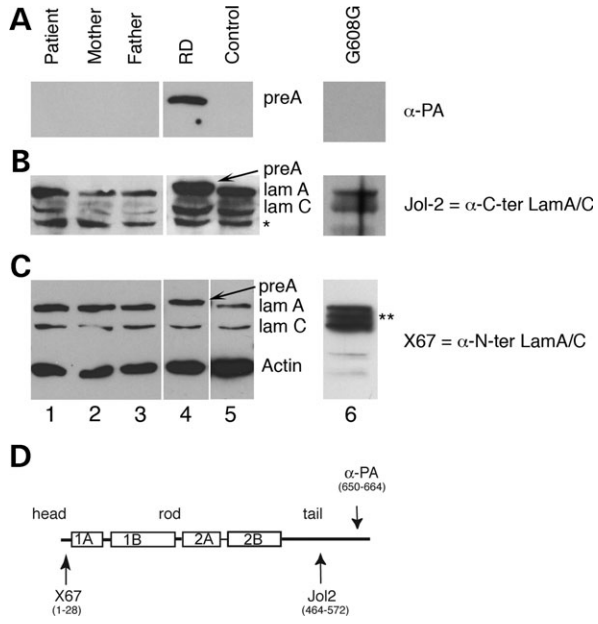

Figure 7. Immunoblotting for A-type lamins in preparations from fibroblasts of the 2-year-old proband (lane 1), the mother (lane 2), the father (lane3), a patient with RD caused by a homozygous c.1085_1086insT mutation in *ZMPSTE24* (lane 4), control fibroblasts (NHDFα) (lane 5) and from a patient with classical HGPS due to a p.G608G mutation (lane 6). Actin was used as a control for protein loading. (**A**) With the prelamin A antibody, a distinct band could be detected in the RD patient (lane 4). The same band was also seen with the Jol-2 and X67 antibodies. (**B**) With the Jol-2 antibody, protein bands corresponding to lamins A and C could be detected. Below the band corresponding to lamin C, an additional band identifying a 46 kDa proteolytic fragment containing the C-terminal end of lamin A/C was found (asterisk), not seen with the X67 antibody. (**C**) In the protein sample of the patient with classical HGPS, an additional band representing progerin (double asterisk) could be detected with the X67 antibody. (**D**) Schematic representation of the epitopes recognized by the different antibodies used in the immunoblotting assay.

in the vicinity of the K542 residue that has been implicated in a recessive progeria syndrome (22). Both mutations affect the C-terminal domain of A-type lamins and are close to residue R527, implicated in MAD type A (p.R527H) (20). Neither mutation gives rise to a clinical laminopathy when occurring in the heterozygous state. However, ~6% of all fibroblasts in the mother exhibited abnormal nuclei with honeycomb patterns and budding. The fact that similar or even smaller percentages of honeycomb figures were found in patients with a full-blown laminopathy (23) suggests that these nuclear dysmorphisms are not necessarily associated with overt disease.

The p.T528M mutation inherited from the healthy father has already been described in a heterozygous compound combination with the p.S583L mutation, causing a severe FPLD (24). The heterozygous p.T528M mutation was found to cause mild metabolic changes without clinical features of a laminopathy. However, another amino acid substitution at the same position (p.T528K) has been associated with EDMD (18). We suggest that an amino acid substitution to lysine (p.T528K), which results in introduction of a positive charge in an enfolded amino acid, perturbs the structure of the globular domain to a greater extent than the T528M mutation. Significant clinical heterogeneity associated with change of a single amino acid has also been described for other laminopathies (25,26). In the present case, the father showed no clinical phenotype, although again ~6% of his fibroblasts exhibited abnormal nuclei with a honeycomb pattern. Of our patients' fibroblasts, on average 36% showed dysmorphic nuclei with honeycomb pattern and budding. The amount of dysmorphic nuclei encountered likely reflects the extent of lamina destabilization.

Interestingly, in the nuclei of our patient, we could not detect the multi-lobulation suggested to be typical for HGPS (27,28). In addition, the loss of lamin B1 within the nuclear protrusions as well as the honeycomb figures that we found in our patient do not seem to be typical for classical HGPS (28). The large fraction of dysmorphic nuclei in general and of the honeycomb figures in particular contrasts with classical HGPS and might reflect a different pathogenetic mechanism with similar or identical clinical features.

Recent work has shown that FTIs are able to ameliorate the nuclear phenotype of human fibroblasts carrying a heterozygous missense mutation, i.e. p.R644C or p.E578V, each associated with a progeroid phenotype (15). Consistent with these findings, treatment of our patients' fibroblasts with an HMG-CoA reductase inhibitor (lovastatin) abolishing farnesyl synthesis improved the nuclear morphology based on a more ovoid appearance of the nuclei with a reduction in the amount of honeycomb structures and blebs. Whether this morphological rescue is also a functional one needs further investigation. FTI and HMG-CoA reductase inhibitors reduce the level of mature lamin A, which could affect mechanical strength (29), mechanotransduction (30) as well as gene regulation. In this respect, it would be interesting to look for normalization of the gene expression profiles in HGPS after treatment with FTI/HMG-CoA reductase inhibitors.

Downloaded from https://academic.oup.com/hmg/article/15/16/2509/645147 by guest on 24 April 2024

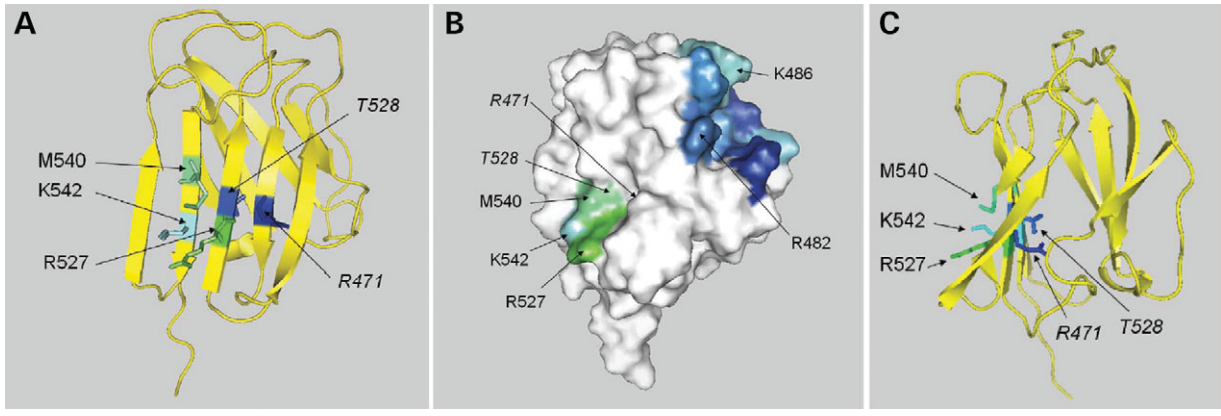

Figure 8. Three-dimensional structure of the C-terminal Ig-fold (411–553) of A-type lamins as determined by NMR spectroscopy. (**A**) The affected residue T528 is located on β-strand 8 next to residue R527 involved in MAD. Its side chain is buried in the hydrophobic core of the domain. Residue M540 is solvent accessible and located on β-strand 9 of the same β-sheet, close to residue K542 associated with a progeria syndrome. Residue R471 implicated in a progeria syndrome is located on β-strand 4. Colors correspond to the degree of conservation of the residue in A- and B-type lamins: from dark blue, highly conserved, to green, less conserved. (**B**) Solid three-dimensional representation. On the progeria-related surface, residues M540 as well as residues R527 and K542 are conserved in A-type lamins (from fish to human) but not in B-type lamins and are therefore depicted in green. Residues T528 and R471 (depicted in italic) are mostly conserved in all type lamins but they have buried side chains and are thus not seen on the surface of the globular domain. The highly conserved positively charged surface in dark blue is the region commonly affected in FPLD (e.g. residues R482 and K486). (**C**) Profile of the C-terminal Ig-fold domain clearly illustrating that residues R471 and T528 are buried in the structure, whereas residues M540, K542 and R527 are facing the solvent.

Interestingly, inhibition of farnesylation resulted in prelamin A accumulation in well-defined tubule-like structures and annular nuclear membrane plaques rather than in random aggregations. Electron microscopy of lovastatin-treated patient nuclei revealed these structures to be nuclear membrane invaginations surrounded by heterochromatin. The co-localization of prelamin A-labelled structures with heterochromatin clumps may imply a putative role for prelamin A in chromatin remodeling as was suggested earlier (31). A similar localization pattern as in nuclear membrane invaginations/cable-like structures has been described for progerin in HGPS fibroblasts (32). This organization in nuclear membrane invaginations, some of which are projecting throughout the full thickness of the nucleus, supports the previously reported phenomenon of donut-shaped nuclei noticed after FTI treatment of human control fibroblasts (14). We presume that the CxxM-motif preserved by farnesylation inhibition is involved in the formation of these well-organized nuclear membrane invaginations and annular nuclear membrane plaques, as previous studies have considered the farnesylated cysteine of the post-translationally processed CxxM motif in B-type lamins to be one of the triggers for nuclear membrane growth (33). Hence, the large number of nuclear membrane invaginations per nucleus encountered in the RD fibroblasts may be due to the farnesylated CxxM-motif that is retained due to lack of active zmpste24 enzyme. Although the inhibition of farnesyl synthesis preserves the CaaX-motif and prohibits its farnesylation, this non-farnesylated CxxM-motif may be sufficient to induce nuclear membrane growth, supported by the large increase in the number of tubules per nucleus in the 2-year-old patient after farnesylation inhibition (Table 1). In addition, farnesylation inhibition did not significantly alter the number of nuclear membrane invaginations observed in the RD patient (Table 1) or the HGPS patient (data not shown). From what stated earlier, we hypothesize that lamins retaining the CaaX-motif independent of the presence of the isoprenyl group become incorporated in the lamina, leading to nuclear membrane growth with the formation of nuclear invaginations subsequently. Although the viability of patient and control fibroblasts was largely unaffected by the 18 h incubation with 40 μM lovastatin, long-term effects of farnesylation inhibition by lovastatin could not be studied due to an increased toxicity. Similar nuclear membrane invaginations could be detected with the prelamin A antibody in fibroblasts from the index and control patients after treatment with the FTI-277 (20 μM) that was reported to exhibit beneficial effects on nuclear morphology in HGPS fibroblasts (32). The number of nuclear membrane invaginations increased significantly after FTI treatment (Table 1). Recently, cable-like structures identical to the nuclear invaginations we observed could be detected in senescent cells in HGPS fibroblast cultures and an association between the formation of these nuclear structures and senescence was suggested (32). In that perspective, the beneficial effect of farnesylation inhibitors in the treatment of HGPS may be questioned, in particular in the case of the patient described in this manuscript.

Recent FRET studies show the wild-type polymerization of A- and B-type lamins to be lost in the presence of progerin (34) and support the idea that nuclear lamina destabilization may be a key event in the pathogenesis of progeroid laminopathies. The combination of a mutation in the area around residue K542, previously implicated in progeria, with a beta-strand destabilizing mutation at the hydrophobic residue T528 in the same region (Fig. 8) might well affect lamin polymerization and nuclear lamina structure. Consistent with our findings, a previously reported heterozygous compound mutation, affecting two closely positioned residues R527 and R471 located in the same progeria-related hot spot, was also found to cause a progeria syndrome (21). It is clear that all lamin A/C proteins of our patient are modified in the progeria-related hot spot of the molecules, either by one or the other mutation. Thus, interactions crucial for the structure

Downloaded from https://academic.oup.com/hmg/article/15/16/2509/645147 by guest on 24 April 2024

of the nuclear lamina and mediated by this region conserved in A-type lamins are most probably affected. This could alter the mechanical stiffness of these nuclei, as previously shown for cells lacking A-type lamins (29). In addition, the formation of the intranuclear lamin network could be disrupted, thus affecting the intra-nuclear processes in which lamins are involved, such as transcription, DNA replication and DNA repair (12,35). Furthermore, A-type lamins are required for the stability, localization and activity of the retinoblastoma protein (pRB) which is an important regulator of cell proliferation and differentiation (36). Hence, abnormal interaction between mutated A-type lamins and pRB could lead to a deficient differentiation of fat and muscle tissue (37). Viewing the role of A-type lamins in downstream signaling of transforming growth factor-β1 (TGF-β1), an accelerated cell turnover leading to premature aging might additionally explain the progeria phenotype (38). A-type lamins were shown to modulate the effect of TGF-β1 on collagen production with an increased level of collagen produced in *LMNA* −/− mouse fibroblasts (38). The latter function of A-type lamins likely explains the increased fibrosis of the heart encountered in patients with a laminopathy (39–41) and in mice modelling HGPS (42) and suggests its contribution to heart failure in patients with *LMNA* mutations.

The defective lamina structure formed in the case of compound heterozygosity should result in a high rate of laminopathy-related nuclear morphologies. Indeed, we found many such abnormalities, including honeycomb patterns, in the cultured fibroblasts of the 2-year-old patient. The parents presented a smaller number of affected nuclei, most likely because less mutant lamin products are available to form abnormal dimers. In the child, all dimers are mutant, resulting in the larger fraction of dysmorphic nuclei. These data, as well as the fact that progerin presumably functions as a dominant negative by interfering with the structure of the nuclear lamina, intranuclear architecture and macromolecular interactions (11), support the hypothesis that only mutations causing severe disturbances of the lamin dimerization/polymerization result in a progeroid phenotype. Examples are p.G608G resulting in a processing defect, mutations within the globular domain important for head-to-tail polymerization and nuclear lamina structure, as well as mutations that seriously affect the α-helical structure involved in dimerization. The phenotype associated with heterozygous missense mutations therefore greatly depends on their positions in the protein.

In conclusion, we present a heterozygous compound mutation in *LMNA* that causes an apparently typical HGPS without prelamin A accumulation. The disorganization of the NE detected in fibroblasts of the index patient and his parents suggests an important role for the progeria hot-spot domain in the assembly of nuclear lamins. Our data support the contribution of abnormal polymerization to the pathogenesis of HGPS and indicate that progeria can develop in the absence of progerin or prelamin A accumulation. If prelamin A accumulation occurs, it is well organized at the nuclear rim, in intra/trans-nuclear nuclear membrane invaginations and in annular nuclear membrane plaques. Interestingly, the CaaX-motif of lamins is sufficient to induce nuclear membrane growth, independent of its farnesylation.

MATERIALS AND METHODS

Patient and controls

The proband is the 2-year-old son of healthy unrelated parents of Dutch descent. He has one younger sister, aged 1 month, who is clinically unaffected.

From the proband, parents and sister, blood samples were collected in tubes containing ethylenediamine tetraacetic acid (EDTA). From the proband and his parents, a skin biopsy was performed for further immunohistochemical studies and fibroblast culturing. The parents provided informed consent for inclusion in this study. Control blood samples were from 200 unrelated Dutch individuals.

Mutation analysis

Genomic DNA was extracted from whole blood by standard procedures using the Wizard genomic DNA purification kit (Promega, Leiden, The Netherlands). The coding exons of *LMNA*, including the splice junctions, were amplified by PCR. PCR reactions (50 μl) contained 1× Taq buffer (Invitrogen, Groningen, The Netherlands), 0.2 mM dNTPs, 100 ng of each primer and 1.0 U Taq DNA polymerase (Invitrogen). PCR conditions were: 30 s 94°C, 30 s 62°C, 60 s 72°C for 35 cycles, initiated by 90 s at 94°C and terminated by 420 s at 72°C. PCR products were purified in 50 μl elution buffer (Tris 10 mM, pH 8.0) with a MultiScreen-PCR filter plate (Millipore) or Qiagen PCR purification kit (Qiagen Benelux B.V.). Subsequently, 1 μl was directly sequenced with the Big dye terminator V1.1 cycle sequencing kit (Applied Biosystems, Fostercity, CA, USA) using the PCR primers according to the specifications of the manufacturer (all primer sequences are available upon request). Sequence analysis was performed with Vector NTI software (Informax, Inc.).

Immunohistochemical staining of cultured patient fibroblasts

Fibroblasts were cultured from a skin biopsy and grown on glass cover slips in 12-well culture plates with DMEM-F12 (Cambrex, England), 10% fetal calf serum and antibiotics in a 1:100 dilution (penicillin–streptomycin; GIBCO, Cat. no. 15140–148). After reaching 80% confluency, the cells were fixed with 4% formaldehyde in phosphate-buffered saline (PBS) pH 7.4 for 15 min, followed by permeabilization in 0.1% Triton X-100 for 10 min at room temperature (RT). Cells stained with the LN43 antibody were fixed in methanol at −20°C for 10 min. Primary antibodies (view list subsequently) diluted in PBS containing 3% bovine serum albumin (BSA) were applied onto the cells for 1 h. After extensive washing in PBS, secondary antibodies were applied for 1 h at RT. Secondary antibodies used are FITC-conjugated rabbit anti-mouse Ig (1:100, DAKO, Glostrup, Denmark) or FITC-conjugated swine anti-rabbit Ig (1:80, DAKO, Glostrup, Denmark). Secondary antibodies were also diluted in PBS with 3% BSA. After three final washing steps (each 5 min) in PBS, slides were mounted in 90% glycerol, 0.02 M Tris–HCl pH 8.0, 0.8% NaN_3 and 2% 1,4-di-azobicyclo-(2,2,2)-octane (DABCO; Merck, Darmstadt, Germany) containing 0.5 μg/ml PI.

Downloaded from https://academic.oup.com/hmg/article/15/16/2509/645147 by guest on 24 April 2024

Primary antibodies used for immunofluorescence studies

(1) 133A2 (mouse IgG3) [a kind gift from Dr Y. Raymond (Montreal, Canada) and distributed by MUbio Products BV, Maastricht, The Netherlands] recognizes lamin A and AΔ10, reacting with an epitope present in the aminoacid sequence between residues 598 and 611 (43). Dilution used for immunohistochemistry: 1/100.
(2) RalC (MUbio Products BV) is an affinity-purified rabbit polyclonal antibody directed against the C-terminal sequence VSGSRR (position 567–572) of human lamin C (44). Dilution used for immunohistochemistry: 1/20.
(3) Jol-2 (mouse IgG1) (MUbio Products BV) reacting with an epitope in the C-terminal domain (amino acids 464–572) of lamin A, AΔ10 and C (45). Dilution used for immunohistochemistry: 1/20; for immunoblotting: 1/1000.
(4) 119D5-F1 (mouse IgG1) was kindly provided by Dr Y. Raymond (Montreal, Canada). This antibody is directed against an epitope, located C-terminus of the caspase cleavage site of lamin B1, and reacts with an epitope located C-terminus of residue 231 in lamin B1 (43,46). Dilution used for immunohistochemistry: 1/100.
(5) Lamin B1 is an affinity-purified rabbit polyclonal antibody to lamin B1, kindly provided by Dr J.C. Courvalin (INSERM, Paris, France) (47). Dilution used for immunohistochemistry: 1/100.
(6) LN43 (mouse IgG1) recognizes lamin B2 and does not cross-react with lamin B1 or A-type lamins (48). The antibody was kindly provided by Dr Birgit Lane (Dundee, UK). LN43 was used as undiluted culture supernatant. Dilution used for immunohistochemistry: 1/5.
(7) NCL-Emerin (mouse IgG1, Novocastra) clone 4G5 directed against a 222 amino acid fragment near the N-terminus of the emerin protein (49,50). Dilution used for immunohistochemistry: 1/50.
(8) A polyclonal rabbit antibody α-PA kindly provided by Dr Sinensky, synthesized against the 15 amino acids of prelamin A, which are proteolytically removed during the farnesylation-dependent processing of this molecule (51). This antibody will be referred to as the prelamin A antibody. Dilution used for immunohistochemistry: 1/200; for immunoblotting: 1/250.
(9) X67 (mouse IgG1) kindly provided by Dr G. Krohne (Würzburg, Germany) recognizing amino acids 1–28 at the N-terminus of lamins A, AΔ10 or C. Dilution used for immunoblotting: 1/50.
(10) β-actin (mouse IgG1, Sigma clone AC-15) recognizing a slightly modified β-cytoplasmic actin N-terminal peptide. Dilution used for immunoblotting: 1/5000.

Fibroblast cultures and lovastatin/FTI-277 treatment

From the index patient, his parents, a patient with HGPS due to a p.G608G mutation in *LMNA* and a patient with RD due to homozygous c.1085_1086insT truncating mutations in *ZMPSTE24*, fibroblasts were obtained by a skin biopsy. In addition, a human control fibroblast cell line NHDFα was used.

Fibroblasts were cultured on glass cover slips in 12-well culture plates up to 50% confluence with DMEM-F12 (Cambrex), 10% fetal calf serum and antibiotics in a 1:100 dilution (penicilline-streptomycine; GIBCO, Cat. no. 15140–148). The HMG-CoA reductase inhibitor lovastatin (Merck, Rahway, NJ, USA) or the FTI-277 (Calbiochem, Merck, VWR International BV, The Netherlands) was added to the culture medium at a 40 and 20 μM concentration, respectively. After 18 h, the cells were fixed with 4% formaldehyde in PBS for 15 min and stained with the prelamin A and Jol-2 antibodies as described above.

Viability assays

Fibroblasts of the index patient were cultured on glass cover slips in 12-well culture plates up to 50% confluence with DMEM-F12 (Cambrex), 10% fetal calf serum and antibiotics in a 1:100 dilution (penicillin–streptomycin; GIBCO, Cat. no. 15140–148). The HMG-CoA reductase inhibitor lovastatin (Merck) was added to the culture medium at a 5, 10, 20 and 40 μM concentration. After 18 and 42 h, PI was added to the culture medium for about 10 min at a concentration of 10 μg/ml. The fraction of PI-positive cells fixed at the bottom of the culture well and those detected in a cytospin of the culture medium containing the cells that had detached from the bottom were estimated in order to assess the frequency of non-viable cells. In addition, fibroblasts of the index patient and control (NHDFα) were cultured under the same conditions in six-well culture plates and treated with lovastatin (40 μM). PI (10 μg/ml) was added to the culture medium after 18 and 42 h of lovastatin treatment and cells were studied in an FACS assay as previously described (52). A FACSort (Becton Dickinson, Sunnyvale, CA, USA) flow cytometer equipped with an argon ion laser and a diode laser was used. Excitation was performed at 488 nm, and the emission filter used was 600 LP (red). A minimum of 10.000 cells per sample were analyzed. PI signals were recorded as logarithmic amplified data. Data analysis was performed using the CellQuest 3.1 software (Becton Dickinson, San Jose, CA, USA).

Confocal laser scanning microscopy

Fluorescent samples were imaged using a Bio-Rad MRC600 confocal microscope (Bio-Rad Laboratories Ltd, Hemel Hempstead, UK), equipped with an air-cooled Argon–Krypton mixed gas laser and mounted onto an Axiophote microscope (Zeiss), using oil-immersion objectives (40×, NA $\frac{1}{4}$ 3D1.3 or 63×, NA$\frac{1}{4}$ 3D1.4). The microscope was used in the dual parameter set-up, according to manufacturer's specifications, using dual wavelength excitation at 488 and 568 nm. Emission spectra were separated by the standard sets of dichroic mirrors and barrier filters. Optical sections were recorded in the Kalman filtering mode using 5–8 scans for each picture. Z-series were generated by collecting a stack consisting of optical sections using a step size of 0.18 μm in the *z*-direction. The Huygens System image restoration software (Scientific Volume Imaging B.V., Hilversum, The Netherlands) was used to improve the effective resolution of some of the confocal images and to reduce background noise. For this purpose, a maximum likelihood estimation algorithm (53) was used.

Downloaded from https://academic.oup.com/hmg/article/15/16/2509/645147 by guest on 24 April 2024

Electron Microscopy

For transmission electron microscopy, cell cultures were fixed in 3% glutaraldehyde buffered with 90 mM KH_2PO_4 (pH 7.4). After post-fixation with 2% OsO_4 (Agar Scientific, Stansted, UK) in 0.1 M veronalacetate buffer followed by impregnation in 1% uranylacetate (Ladd Research Industries, Burlington, VT, USA) in 0.1 M veronalacetate (pH 5.2), the cell cultures were dehydrated in graded series of ethanol and routinely embedded in Epon (Ladd Research Industries). Ultrathin sections were counterstained with uranium acetate and lead citrate prior to examination in a Philips CM100 electron microscope.

Sample preparation for gel electrophoresis and immunoblotting

Cells were grown in a 175 cm^2 culture flask and harvested, after one wash with PBS containing 0.5 mM protease blocking agent phenylmethylsulfonyl chloride (PMSC) (Merck), by scraping with a rubber police man in 200 μl ice-cold lysis buffer (containing 62.5 mM Tris–HCl, pH 6.8, 12.5% glycerol, 2% NP-40, 2.5 mM PMSC, 1.25 mM EDTA, 12.5 μg/ml leupeptin and 50 μg/ml trasylol). Cell suspensions were kept on ice for 30 min, diluted 1:1 with SDS-sample buffer (62.5 mM Tris–HCl, pH 6.8, 2.3% SDS, 10% glycerol, 5% β-mercapto-ethanol and 0.05% Bromophenol blue), boiled for 4 min and stored at −20°C until further use.

Gel electrophoresis and immunoblotting

One-dimensional SDS–polyacrylamide gel electrophoresis in 10% polyacrylamide (Bio-Rad Laboratories) slabgels was performed as described by Laemmli (54). Gels were run on the Mini-Protean II system from Bio-Rad laboratories for ∼45 min at 200 V. Immunoblotting was performed according to Towbin *et al*. (55) using a Mini Trans-Blot cell from Bio-Rad laboratories at 100 V for 1 h. A Coomassie staining of the gel as well as actin immunostaining of the blot was performed to assess the amount of protein loaded onto the gel.

Proteins were blotted onto nitrocellulose membranes (BA85, Schleicher and Schüll, Dassel, Germany). The membranes were pre-incubated in blocking solution (PBS/ 0.5% Triton X-100 with 5% non-fat dry milk) followed by 1 h incubation with mouse antibody Jol-2 (dilution 1:1000), X67 (dilution 1:50) and rabbit polyclonal antibody prelamin A (dilution: 1/250). As secondary antibody, peroxidase-conjugated rabbit anti-mouse Ig (DAKO/ITK) (dilution 1/10 000) and peroxidase-conjugated swine anti-rabbit Ig (DAKO/ITK) (dilution 1/5000) were used. Peroxidase activity was detected by chemiluminescence (ECL West Dura Pierce, Rockford, IL, USA) and visualized on RX Fuji medical X-ray films (Fuji, Tokyo, Japan).

ACKNOWLEDGEMENTS

The authors wish to thank Dr Fons Verheyen for the electron microscopic studies on the cell cultures described, Mrs I.C. van Kesteren (Elkerliek Hospital, Helmond) and Mrs H. Claahsen-van der Grinten (Radboud University Nijmegen Medical Centre, Nijmegen) for clinical support, Dr Jean-Claude Courvalin (INSERM, Institut Jacques Monod, Paris) for kindly providing the antibody to lamin B1, Dr Birgit Lane (Dundee University, Dundee) for kindly providing antibody LN43 to lamin B2, Dr Chris Hutchinson (Durham University, Durham) for kindly providing antibody Jol-2, Dr Georg Krohne (University of Wuerzburg, Wuerzburg) for kindly providing antibody X67 and Dr Michael S. Sinensky (East Tennessee State University, USA) for kindly providing antibody α-PA to prelamin A. The Netherlands Organization for Scientific Research (NWO, project 901-28-134) is acknowledged for financial support for microscopic equipment and imaging software. This work is supported by a research grant of the University Hospital Maastricht to V.L.R.M.V. M.A.M.v.S. is financially supported by Barrier Therapeutics.

Conflict of Interest statement. The authors declare no conflict of interest.

REFERENCES

1. Csoka, A.B., Cao, H., Sammak, P.J., Constantinescu, D., Schatten, G.P. and Hegele, R.A. (2004) Novel lamin A/C gene (LMNA) mutations in atypical progeroid syndromes. *J. Med. Genet.*, **41**, 304–308.
2. Pollex, R.L. and Hegele, R.A. (2004) Hutchinson–Gilford progeria syndrome. *Clin. Genet.*, **66**, 375–381.
3. De Sandre-Giovannoli, A., Bernard, R., Cau, P., Navarro, C., Amiel, J., Boccaccio, I., Lyonnet, S., Stewart, C.L., Munnich, A., Le Merrer, M. *et al*. (2003) Lamin a truncation in Hutchinson–Gilford progeria. *Science*, **300**, 2055.
4. Eriksson, M., Brown, W.T., Gordon, L.B., Glynn, M.W., Singer, J., Scott, L., Erdos, M.R., Robbins, C.M., Moses, T.Y., Berglund, P. *et al*. (2003) Recurrent *de novo* point mutations in lamin A cause Hutchinson–Gilford progeria syndrome. *Nature*, **423**, 293–298.
5. Zastrow, M.S., Vlcek, S. and Wilson, K.L. (2004) Proteins that bind A-type lamins: integrating isolated clues. *J. Cell Sci.*, **117**, 979–987.
6. Goldman, R.D., Gruenbaum, Y., Moir, R.D., Shumaker, D.K. and Spann, T.P. (2002) Nuclear lamins: building blocks of nuclear architecture. *Genes Dev.*, **16**, 533–547.
7. Burke, B. and Stewart, C.L. (2002) Life at the edge: the nuclear envelope and human disease. *Nat. Rev. Mol. Cell Biol.*, **3**, 575–585.
8. Agarwal, A.K., Fryns, J.P., Auchus, R.J. and Garg, A. (2003) Zinc metalloproteinase, ZMPSTE24, is mutated in mandibuloacral dysplasia. *Hum. Mol. Genet.*, **12**, 1995–2001.
9. Navarro, C.L., De Sandre-Giovannoli, A., Bernard, R., Boccaccio, I., Boyer, A., Genevieve, D., Hadj-Rabia, S., Gaudy-Marqueste, C., Smitt, H.S., Vabres, P. *et al*. (2004) Lamin A and ZMPSTE24 (FACE-1) defects cause nuclear disorganization and identify restrictive dermopathy as a lethal neonatal laminopathy. *Hum. Mol. Genet.*, **13**, 2493–2503.
10. Shackleton, S., Smallwood, D.T., Clayton, P., Wilson, L.C., Agarwal, A.K., Garg, A. and Trembath, R.C. (2005) Compound heterozygous ZMPSTE24 mutations reduce prelamin A processing and result in a severe progeroid phenotype. *J. Med. Genet.*, **42**, e36.
11. Reddel, C.J. and Weiss, A.S. (2004) Lamin A expression levels are unperturbed at the normal and mutant alleles but display partial splice site selection in Hutchinson–Gilford progeria syndrome. *J. Med. Genet.*, **41**, 715–717.
12. Scaffidi, P. and Misteli, T. (2005) Reversal of the cellular phenotype in the premature aging disease Hutchinson–Gilford progeria syndrome. *Nat. Med.*, **11**, 440–445.
13. Capanni, C., Mattioli, E., Columbaro, M., Lucarelli, E., Parnaik, V.K., Novelli, G., Wehnert, M., Cenni, V., Maraldi, N.M., Squarzoni, S. *et al*. (2005) Altered pre-lamin A processing is a common mechanism leading to lipodystrophy. *Hum. Mol. Genet.*, **14**, 1489–1502.
14. Glynn, M.W. and Glover, T.W. (2005) Incomplete processing of mutant lamin A in Hutchinson–Gilford progeria leads to nuclear abnormalities, which are reversed by farnesyltransferase inhibition. *Hum. Mol. Genet.*, **14**, 2959–2969.

Downloaded from https://academic.oup.com/hmg/article/15/16/2509/645147 by guest on 24 April 2024

15. Toth, J.I., Yang, S.H., Qiao, X., Beigneux, A.P., Gelb, M.H., Moulson, C.L., Miner, J.H., Young, S.G. and Fong, L.G. (2005) Blocking protein farnesyltransferase improves nuclear shape in fibroblasts from humans with progeroid syndromes. *Proc. Natl Acad. Sci. USA*, **102**, 12873–12878.
16. Yang, S.H., Bergo, M.O., Toth, J.I., Qiao, X., Hu, Y., Sandoval, S., Meta, M., Bendale, P., Gelb, M.H., Young, S.G. *et al*. (2005) Blocking protein farnesyltransferase improves nuclear blebbing in mouse fibroblasts with a targeted Hutchinson–Gilford progeria syndrome mutation. *Proc. Natl Acad. Sci. USA*, **102**, 10291–10296.
17. Burke, B., Tooze, J. and Warren, G. (1983) A monoclonal antibody which recognises each of the nuclear lamin polypeptides in mammalian cells. *EMBO J.*, **2**, 361–367.
18. Krimm, I., Ostlund, C., Gilquin, B., Couprie, J., Hossenlopp, P., Mornon, J.P., Bonne, G., Courvalin, J.C., Worman, H.J. and Zinn-Justin, S. (2002) The Ig-like structure of the C-terminal domain of lamin A/C, mutated in muscular dystrophies, cardiomyopathy, and partial lipodystrophy. *Structure*, **10**, 811–823.
19. Dhe-Paganon, S., Werner, E.D., Chi, Y.I. and Shoelson, S.E. (2002) Structure of the globular tail of nuclear lamin. *J. Biol. Chem.*, **277**, 17381–17384.
20. Novelli, G., Muchir, A., Sangiuolo, F., Helbling-Leclerc, A., D'Apice, M.R., Massart, C., Capon, F., Sbraccia, P., Federici, M., Lauro, R. *et al*. (2002) Mandibuloacral dysplasia is caused by a mutation in LMNA-encoding lamin A/C. *Am. J. Hum. Genet.*, **71**, 426–431.
21. Cao, H. and Hegele, R.A. (2003) LMNA is mutated in Hutchinson–Gilford progeria (MIM 176670) but not in Wiedemann–Rautenstrauch progeroid syndrome (MIM 264090). *J. Hum. Genet.*, **48**, 271–274.
22. Plasilova, M., Chattopadhyay, C., Pal, P., Schaub, N.A., Buechner, S.A., Mueller, H., Miny, P., Ghosh, A. and Heinimann, K. (2004) Homozygous missense mutation in the lamin A/C gene causes autosomal recessive Hutchinson–Gilford progeria syndrome. *J. Med. Genet.*, **41**, 609–614.
23. Vigouroux, C., Auclair, M., Dubosclard, E., Pouchelet, M., Capeau, J., Courvalin, J.C. and Buendia, B. (2001) Nuclear envelope disorganization in fibroblasts from lipodystrophic patients with heterozygous R482Q/W mutations in the lamin A/C gene. *J. Cell Sci.*, **114**, 4459–4468.
24. Savage, D.B., Soos, M.A., Powlson, A., O'Rahilly, S., McFarlane, I., Halsall, D.J., Barroso, I., Thomas, E.L., Bell, J.D., Scobie, I. *et al*. (2004) Familial partial lipodystrophy associated with compound heterozygosity for novel mutations in the LMNA gene. *Diabetologia*, **47**, 753–756.
25. Caux, F., Dubosclard, E., Lascols, O., Buendia, B., Chazouilleres, O., Cohen, A., Courvalin, J.C., Laroche, L., Capeau, J., Vigouroux, C. *et al*. (2003) A new clinical condition linked to a novel mutation in lamins A and C with generalized lipoatrophy, insulin-resistant diabetes, disseminated leukomelanodermic papules, liver steatosis, and cardiomyopathy. *J. Clin. Endocrinol. Metab.*, **88**, 1006–1013.
26. Kirschner, J., Brune, T., Wehnert, M., Denecke, J., Wasner, C., Feuer, A., Marquardt, T., Ketelsen, U.P., Wieacker, P., Bonnemann, C.G. *et al*. (2005) p.S143F mutation in lamin A/C: a new phenotype combining myopathy and progeria. *Ann. Neurol.*, **57**, 148–151.
27. Goldman, R.D., Shumaker, D.K., Erdos, M.R., Eriksson, M., Goldman, A.E., Gordon, L.B., Gruenbaum, Y., Khuon, S., Mendez, M., Varga, R. *et al*. (2004) Accumulation of mutant lamin A causes progressive changes in nuclear architecture in Hutchinson–Gilford progeria syndrome. *Proc. Natl Acad. Sci. USA*, **101**, 8963–8968.
28. Paradisi, M., McClintock, D., Boguslavsky, R.L., Pedicelli, C., Worman, H.J. and Djabali, K. (2005) Dermal fibroblasts in Hutchinson–Gilford progeria syndrome with the lamin A G608G mutation have dysmorphic nuclei and are hypersensitive to heat stress. *BMC Cell Biol.*, **6**, 27.
29. Broers, J.L.V., Peeters, E.A., Kuijpers, H.J., Endert, J., Bouten, C.V., Oomens, C.W., Baaijens, F.P. and Ramaekers, F.C.S. (2004) Decreased mechanical stiffness in LMNA−/− cells is caused by defective nucleo-cytoskeletal integrity: implications for the development of laminopathies. *Hum. Mol. Genet.*, **13**, 2567–2580.
30. Lammerding, J., Schulze, P.C., Takahashi, T., Kozlov, S., Sullivan, T., Kamm, R.D., Stewart, C.L. and Lee, R.T. (2004) Lamin A/C deficiency causes defective nuclear mechanics and mechanotransduction. *J. Clin. Invest.*, **113**, 370–378.
31. Maraldi, N.M., Lattanzi, G., Capanni, C., Columbaro, M., Merlini, L., Mattioli, E., Sabatelli, P., Squarzoni, S. and Manzoli, F.A. (2006) Nuclear envelope proteins and chromatin arrangement: a pathogenic mechanism for laminopathies. *Eur. J. Histochem.*, **50**, 1–8.
32. McClintock, D., Gordon, L.B. and Djabali, K. (2006) Hutchinson–Gilford progeria mutant lamin A primarily targets human vascular cells as detected by an anti-Lamin A G608G antibody. *Proc. Natl Acad. Sci. USA*, **103**, 2154–2159.
33. Prufert, K., Vogel, A. and Krohne, G. (2004) The lamin CxxM motif promotes nuclear membrane growth. *J. Cell Sci.*, **117**, 6105–6116.
34. Delbarre, E., Tramier, M., Coppey-Moisan, M., Gaillard, C., Courvalin, J.C. and Buendia, B. (2006) The truncated prelamin A in Hutchinson–Gilford progeria syndrome alters segregation of A-type and B-type lamin homopolymers. *Hum. Mol. Genet.*, **15**, 1113–1122.
35. Hutchison, C.J. (2002) Lamins: building blocks or regulators of gene expression? *Nat. Rev. Mol. Cell Biol.*, **3**, 848–858.
36. Johnson, B.R., Nitta, R.T., Frock, R.L., Mounkes, L., Barbie, D.A., Stewart, C.L., Harlow, E. and Kennedy, B.K. (2004) A-type lamins regulate retinoblastoma protein function by promoting subnuclear localization and preventing proteasomal degradation. *Proc. Natl Acad. Sci. USA*, **101**, 9677–9682.
37. Classon, M., Kennedy, B.K., Mulloy, R. and Harlow, E. (2000) Opposing roles of pRB and p107 in adipocyte differentiation. *Proc. Natl Acad. Sci. USA*, **97**, 10826–10831.
38. Van Berlo, J.H., Voncken, J.W., Kubben, N., Broers, J.L.V., Duisters, R., van Leeuwen, R.E., Crijns, H.J., Ramaekers, F.C.S., Hutchison, C.J. and Pinto, Y.M. (2005) A-type lamins are essential for TGF-beta1 induced PP2A to dephosphorylate transcription factors. *Hum. Mol. Genet.*, **14**, 2839–2849.
39. Arbustini, E., Pilotto, A., Repetto, A., Grasso, M., Negri, A., Diegoli, M., Campana, C., Scelsi, L., Baldini, E., Gavazzi, A. *et al*. (2002) Autosomal dominant dilated cardiomyopathy with atrioventricular block: a lamin A/C defect-related disease. *J. Am. Coll. Cardiol.*, **39**, 981–990.
40. Fatkin, D., MacRae, C., Sasaki, T., Wolff, M.R., Porcu, M., Frenneaux, M., Atherton, J., Vidaillet, H.J., Jr, Spudich, S., De Girolami, U. *et al*. (1999) Missense mutations in the rod domain of the lamin A/C gene as causes of dilated cardiomyopathy and conduction-system disease. *N. Engl. J. Med.*, **341**, 1715–1724.
41. Sebillon, P., Bouchier, C., Bidot, L.D., Bonne, G., Ahamed, K., Charron, P., Drouin-Garraud, V., Millaire, A., Desrumeaux, G., Benaiche, A. *et al*. (2003) Expanding the phenotype of LMNA mutations in dilated cardiomyopathy and functional consequences of these mutations. *J. Med. Genet.*, **40**, 560–567.
42. Mounkes, L.C., Kozlov, S., Hernandez, L., Sullivan, T. and Stewart, C.L. (2003) A progeroid syndrome in mice is caused by defects in A-type lamins. *Nature*, **423**, 298–301.
43. Hozak, P., Sasseville, A.M., Raymond, Y. and Cook, P.R. (1995) Lamin proteins form an internal nucleoskeleton as well as a peripheral lamina in human cells. *J. Cell Sci.*, **108**, 635–644.
44. Venables, R.S., McLean, S., Luny, D., Moteleb, E., Morley, S., Quinlan, R.A., Lane, E.B. and Hutchison, C.J. (2001) Expression of individual lamins in basal cell carcinomas of the skin. *Br. J. Cancer*, **84**, 512–519.
45. Dyer, J.A., Kill, I.R., Pugh, G., Quinlan, R.A., Lane, E.B. and Hutchison, C.J. (1997) Cell cycle changes in A-type lamin associations detected in human dermal fibroblasts using monoclonal antibodies. *Chromosome Res.*, **5**, 383–394.
46. Machiels, B.M., Broers, J.L., Raymond, Y., de Ley, L., Kuijpers, H.J., Caberg, N.E. and Ramaekers, F.C. (1995) Abnormal A-type lamin organization in a human lung carcinoma cell line. *Eur. J. Cell Biol.*, **67**, 328–335.
47. Chaudhary, N. and Courvalin, J.C. (1993) Stepwise reassembly of the nuclear envelope at the end of mitosis. *J. Cell Biol.*, **122**, 295–306.
48. Bridger, J.M., Kill, I.R., O'Farrell, M. and Hutchison, C.J. (1993) Internal lamin structures within G1 nuclei of human dermal fibroblasts. *J. Cell Sci.*, **104**, 297–306.
49. Bione, S., Maestrini, E., Rivella, S., Mancini, M., Regis, S., Romeo, G. and Toniolo, D. (1994) Identification of a novel X-linked gene responsible for Emery–Dreifuss muscular dystrophy. *Nat. Genet.*, **8**, 323–327.
50. Nigro, V., Bruni, P., Ciccodicola, A., Politano, L., Nigro, G., Piluso, G., Cappa, V., Covone, A.E., Romeo, G. and D'Urso, M. (1995) SSCP detection of novel mutations in patients with Emery–Dreifuss muscular dystrophy: definition of a small C-terminal region required for emerin function. *Hum. Mol. Genet.*, **4**, 2003–2004.
51. Sinensky, M., Fantle, K. and Dalton, M. (1994) An antibody which specifically recognizes prelamin A but not mature lamin A: application to detection of blocks in farnesylation-dependent protein processing. *Cancer Res.*, **54**, 3229–3232.

Downloaded from https://academic.oup.com/hmg/article/15/16/2509/645147 by guest on 24 April 2024

52. Schutte, B., Henfling, M., Kolgen, W., Bouman, M., Meex, S., Leers, M.P., Nap, M., Bjorklund, V., Bjorklund, P., Bjorklund, B. *et al*. (2004) Keratin 8/18 breakdown and reorganization during apoptosis. *Exp. Cell Res.*, **297**, 11–26.
53. Shepp, L.A. and Vardi, Y. (1982) Maximum likelihood reconstruction for emission tomography. *IEEE Trans. Med. Imag.*, **MI-1**, 113–121.
54. Laemmli, U.K. (1970) Cleavage of structural proteins during the assembly of the head of bacteriophage T4. *Nature*, **227**, 680–685.
55. Towbin, H., Staehelin, T. and Gordon, J. (1979) Electrophoretic transfer of proteins from polyacrylamide gels to nitrocellulose sheets: procedure and some applications. *Proc. Natl Acad. Sci. USA*, **76**, 4350–4354.

Downloaded from https://academic.oup.com/hmg/article/15/16/2509/645147 by guest on 24 April 2024